Research Article | Vol. 30, No. 24 / 21 Nov 2022 / Optics Express 44229
Optics EXPRESS

Ultra-thin deep ultraviolet perfect absorber using an Al/TiO_2/AlN system

YUUSUKE TAKASHIMA,[1,2,*] KENTARO NAGAMATSU,[1,2] MASANOBU HARAGUCHI,[1,2] AND YOSHIKI NAOI[1,2]

[1]*Graduate School of Technology, Industrial and Social Science, Tokushima University, Tokushima 770-8506, Japan*
[2]*Institute of Post-LED Photonics, Tokushima University, 770-8506, Japan*
[*]*takashima@tokushima-u.ac.jp*

Abstract: An ultra-thin perfect absorber for deep ultraviolet light was realized using an Al/TiO_2/AlN system. The TiO_2 thickness was optimized using the Fresnel phasor diagram in complex space to achieve perfect light absorption. As a result of the calculation almost perfect absorption into the TiO_2 film was found, despite the film being much thinner than the wavelength. An optimized Al/TiO_2/AlN system was fabricated, and an average absorption greater than 97% was experimentally demonstrated at wavelengths of approximately 255–280 nm at normal light incidence. Our structure does not require nanopatterning processes, and this is advantageous for low-cost and large-area manufacturing.

1. Introduction

Deep ultraviolet (DUV) light (light at wavelengths (λ) of approximately 200–300 nm) is suitable for biological and chemical sensing applications owing to its strong interaction with molecules in DNAs and harmful gases [1–3]. Sunlight does not include a DUV component, owing to light absorption in the ozone layer [4]. This allows DUV light to achieve a high signal-to-noise (S/N) ratio in sensing applications. Sensitive DUV light detection devices, such as photodetectors that absorb DUV light efficiently and convert its intensity to a photocurrent, are essential for the development sensing applications. A perfect absorber that operates in the DUV region plays a critical role in these devices.

The light absorption rate (A) is defined as 1 − transmittance (T) − reflectivity (R). Perfect absorption occurs when T and R vanish simultaneously. An optical material with a high absorption coefficient attenuates T, but such materials invariably have a highly reflective surface. This is a fundamental issue for the development of perfect optical absorbers. Recently, a new concept for perfect absorbers was proposed using metasurfaces with subwavelength structures [5–20]. The surfaces allow arbitrary control of the optical response, such as R, T, and A at a certain wavelength, via electric or magnetic dipole resonances. Large absorptions have been demonstrated in the ultraviolet to microwave wavelength regions using metal split rings [5–7], helix-metal structures [8], metal-dielectric-metal nanostructures [9–13], nanodisks [14,15], nanoparticles [16–18], and nanoblocks [19,20]. Metals and dielectrics composing meta-structures tend to possess a large extinction coefficient in the DUV region [21–23], weakening such electric and magnetic resonances, thus preventing perfect absorption characteristics.

Perfect absorbers have also been demonstrated by stacking thin films [24–38]. There are many classical examples, such as the Dallenbach absorber [24]. The absorber is composed of a $\lambda/4$ dielectric film with slight loss on a perfect electric conductor (PEC) substrate. Incident light is fully reflected by the PEC and transmitted light vanishes. The $\lambda/4$ dielectric film acts as an anti-reflective coating owing to the destructive interference of the thin film. When T and R vanish simultaneously, the lossy dielectric film fully absorbs the energy of the irradiated light. Based on the concept of destructive interference, several groups recently realized ultra-thin perfect

#474847 https://doi.org/10.1364/OE.474847
Journal © 2022 Received 4 Sep 2022; revised 27 Oct 2022; accepted 1 Nov 2022; published 17 Nov 2022

Optics EXPRESS

absorbers in the visible and infrared regions using highly lossy films of materials such as Ge and Si on metallic grand planes [30–38]. Owing to the moderately large refractive indices (n) and extinction coefficients (k) of these films ($n \approx k$), the Fresnel coefficients of each layer are complex values far from the real axis of the complex space. The phasor diagram of the Fresnel coefficients in the complex space enables destructive interference with a lossy film of much smaller thickness than λ [30–38]. For example, this unique destructive interference demonstrated greater than 98% absorption of light energy into ultra-thin highly lossy films in the visible wavelength region [32]. However, the values of k for typical highly lossy films become too larger in the DUV region than those in longer wavelength regions [21,22]. Such overly large values of k prevent destructive interference owing to the abrupt refractive index contrast to air. Moreover, n and k values of most metals, such as Au, Ag, and Al, decrease in the DUV region owing to their plasma frequencies. Thus, the destructive interference condition is hard to satisfy due to the index mismatch between highly lossy films, metals and incident media (typically air). This is a basic issue for the realization of perfect DUV absorption in ultra-thin, highly lossy films.

In this paper, the problem specific to the DUV region was firstly overcame by the combination of the large n and transparent cover layer and highly lossy but not so large n and k film. We proposed an ultra-thin DUV perfect absorber with an Al/TiO_2 (highly lossy)/AlN (large n) system. The novel combination of Al, TiO_2, and AlN can relax the complex refractive index contrast and successfully achieve destructive interference in ultra-thin lossy film in the DUV region. The calculated phasor diagram in complex space of the Fresnel coefficients indicates that T and R vanish because of multiple reflections in the optimized Al/TiO_2/AlN system owing to the relaxed refractive index contrast at the AlN/TiO_2 interface. The fabricated Al/TiO_2/AlN system achieved 97% absorption in the DUV region (λ = 255–280 nm). Finite-difference time-domain (FDTD) calculation results also clarified that the TiO_2 film fully absorbed most of the incident light energy, despite the TiO_2 thickness being much thinner than the incident wavelength.

2. Design and optimization of AlN/TiO_2/Al ultra-thin DUV absorber

In this section, we explain the design and optimization of the proposed ultra-thin DUV absorber. Figure 1 shows the schematic of the proposed absorber. Our proposed system comprises a transparent cover medium (medium 1), highly lossy ultra-thin film (medium 2), and metal grand plane (medium 3). The complex refractive indices of the cover medium, lossy film, and ground plane are $n_1 + k_1\mathrm{i}$, $n_2 + k_2\mathrm{i}$, and $n_3 + k_3\mathrm{i}$, respectively. For simplicity, we assumed that the thicknesses of the cover medium and grand plane were semi-infinite. The thickness of the lossy film is denoted as h_2. The incident light enters in the direction from medium 1 to medium 3. Here, it is valid to consider that T of the proposed structure becomes zero because of the semi-infinitely thick metal grand plane. In this case, the incident light is confined to the lossy film when reflection is canceled. Consequently, the energy of the incident light is perfectly absorbed by the lossy film.

When incident light enters the proposed structure, it is partially reflected at each interface. Multiple interferences of the reflected light occur inside medium 2. Consequently, the field Fresnel reflection coefficient (r) of the proposed structure is given by:

$$r = \frac{r_{12} + r_{23}\exp(2\beta_2 h_2 \mathrm{i})}{1 + r_{12}r_{23}\exp(2\beta_2 h_2 \mathrm{i})} \tag{1}$$

where r_{ab} indicates the field Fresnel reflection coefficient from medium a to b. The symbol β_2 denotes the vertical wavenumber in medium 2. The cancellation condition of the reflection is obtained when the numerator in Eq. (1) becomes zero. If the refractive index of the lossy medium has a moderately large complex value (i.e., k_2 is close to n_2), the Fresnel reflection coefficient of r_{12} is located in the complex space far from the real axis. A conceptual diagram of cancellation in a complex space is shown in Fig. 2.

Optics EXPRESS

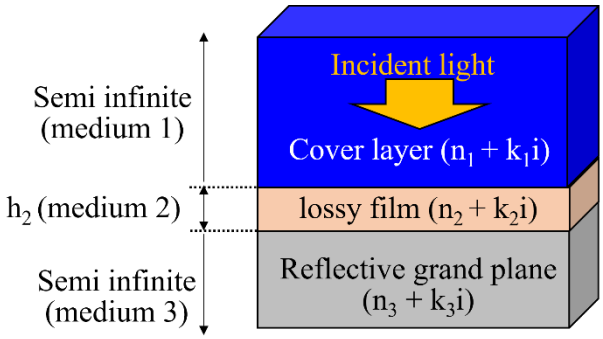

Fig. 1. Proposed DUV absorber with three materials. The thickness of medium 2 is denoted as h_2. The thicknesses of medium 1 (cover layer) and medium 3 (reflective grand plane) are semi-infinite. The incident light enters in the direction from medium 1 to medium 3.

This gives the alternative cancellation condition of R not only near the real axis (this condition corresponds to the traditional anti-reflection coating in Fig. 2) but also in complex space far from the real axis. This condition reduces R to zero, i.e., perfect absorption despite the significantly smaller thickness of the lossy medium [30–38]. However, the imaginary parts of the refractive index of highly lossy materials, such as Si and Ge, are significantly large for DUV wavelengths, for example, the complex refractive indices of Si and Ge are respectively $2.0267 + 4.7117$i and $1.7394 + 3.9881i$ at $\lambda = 270$ nm [22]. When the cover medium is air, the Fresnel reflection cannot be canceled because of the excessively large complex refractive index contrast between air and the lossy medium.

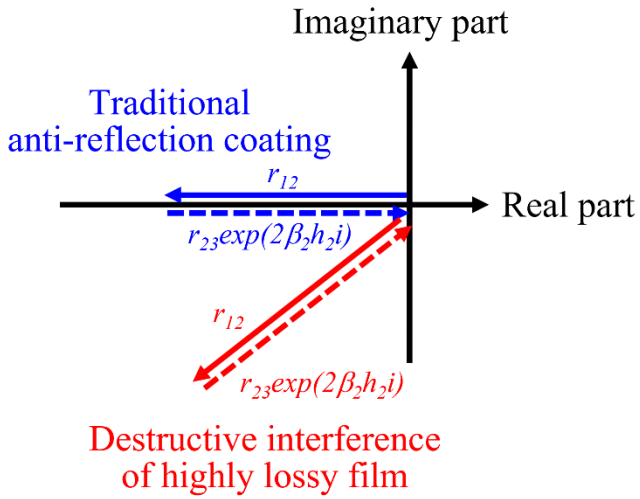

Fig. 2. Conceptual diagram of destructive interference in complex space. The solid and dashed arrows indicate r_{12} and $r_{23}exp(2\beta_2 h_2 i)$, respectively.

To relax the refractive index contrast, we proposed AlN, TiO_2, and Al as the cover layer, highly lossy film, and metal grand plane, respectively. Al is reflective ($0.21643 + 3.1891i$ at $\lambda = 270$ nm, large k and small n) and almost fully reflects the incident light [39]. TiO_2 is highly lossy but has not so large n and k values ($2.8469 + 1.4600i$ at $\lambda = 270$ nm: k is comparable to n) at $\lambda = 200$ to 300 nm wavelength regions whereas it is transparent (k becomes close to zero) at longer wavelength [23]. This dispersion of TiO_2 refractive index is suitable for several

Optics EXPRESS

functionalities, for example visible and infrared blind DUV detection. On the other hand, an AlN has a large n value with high transparency ($2.3344 + 0i$ at $\lambda = 270$ nm: large n and almost zero k) at the broadband wavelength region including DUV wavelength [40]. Thus, the complex Fresnel reflection coefficient r_{12} at the TiO_2/AlN interface becomes the same order amplitude for the multiple reflections inside TiO_2 ($r_{23}exp(2\beta_2 h_2 i)$), and both phases approach to almost anti-phase in complex space. As a result, DUV perfect absorption can be achieved despite of much thinner thickness of TiO_2 than the wavelength. Based on the concept mentioned above, we first optimized the thickness of TiO_2 film.

Figure 3 (a) shows the analytical TiO_2 thickness dependence of the normal reflectivity ($\lambda = 280$ nm) for the Al/TiO_2/air and Al/TiO_2/AlN structures. When the cover layer is air, multiple interferences in the Al/TiO_2/air structure cause reflectivity dips at a TiO_2 thickness of 12 nm. However, 11.6% of the reflectivity remains at the dip owing to the high refractive index contrast between TiO_2 and air. Conversely, a dip in reflectivity of the Al/TiO_2/AlN structure was found at a TiO_2 thickness of 17 nm. The dip reflectivity decreases almost to zero (0.33%), and the reflection is considerably suppressed by the multiple interferences of the Al/TiO_2/AlN structure. To reveal the role of the AlN cover medium in more detail, we calculated the phasor diagram of the field Fresnel reflection coefficients of the Al/TiO_2/air and Al/TiO_2/AlN structure for minimized R conditions. Figure 3 (b) shows the phasor diagram of r_{12} and $r_{23}exp(2\beta_2 h_2 i)$ in the Al/TiO_2/air and Al/TiO_2/AlN structures (see Eq. (1)). The dashed and solid vectors represent the Fresnel reflection coefficients in the Al/TiO_2/air and Al/TiO_2/AlN, respectively. For Al/TiO_2/air structure, the diagram indicates that the reflection amplitude at the TiO_2/air (r_{12}) is larger than the multiple reflections inside the TiO_2 layer (($r_{23}exp(2\beta_2 h_2 i)$)). In contrast, the reflection r_{12} of Al/TiO_2/AlN is almost anti-phase and the same amplitude for its multiple reflections inside the TiO_2 layer ($r_{23}exp(2\beta_2 h_2 i)$). As a result, the reflection of the structure is highly suppressed, and near-perfect absorption (> 99%) can be achieved despite the ultra-thin TiO_2 film.

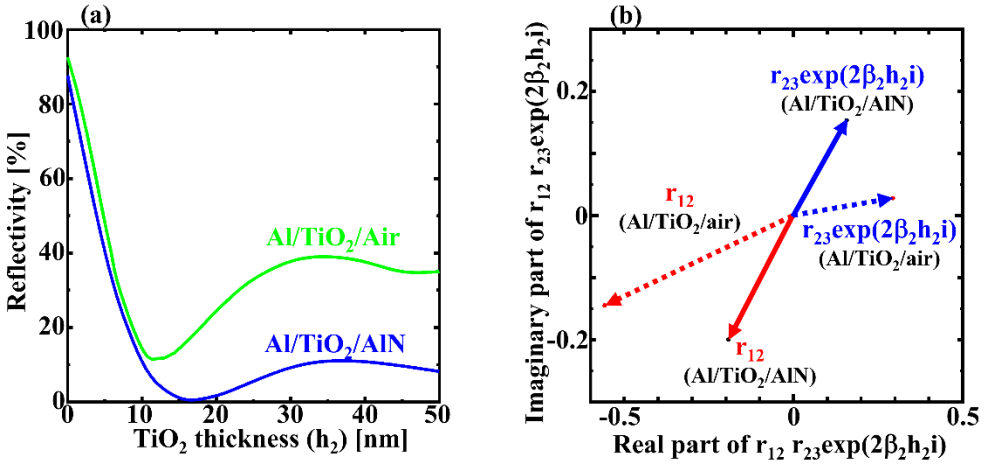

Fig. 3. (a) Calculated TiO_2-thickness dependence of normal reflectivity of Al/TiO_2/air and Al/TiO_2/AlN structure. (b) Phasor diagram of the field Fresnel reflection coefficient in the optimized Al/TiO_2/air and Al/TiO_2/AlN.

Using the FDTD method, we simulated the electromagnetic field distribution within the optimized Al/TiO_2/AlN structure for a perfect absorber, i.e., the thickness of TiO_2 was 17 nm. The FDTD simulation model is shown in Fig. 4. In the simulation, the incident plane wave propagates from the AlN side. We used periodic boundary conditions (PBCs) for the x- and y-directions and assumed that the multilayers infinitely repeat in the in-plane directions. For

Optics EXPRESS

the z-direction, we used perfectly matched layers (PMLs), which did not reflect at the surface and attenuated the amplitude of the light entering the PML. Hence, the thicknesses of AlN and Al were assumed to be semi-infinite. The time and spatial grids in this calculation were 3.33×10^{-12} s and 2 nm, respectively. The reflected light intensity was detected using a power monitor placed behind the light source.

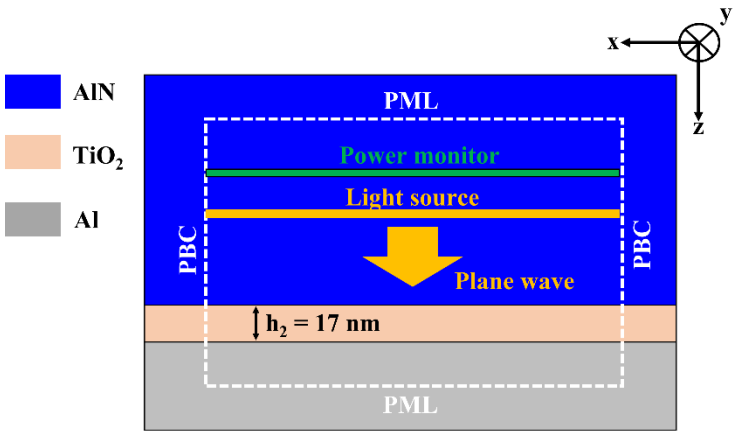

Fig. 4. FDTD field calculation model for the optimized Al/TiO_2/AlN.

Figure 5(a) shows the calculated normal reflection and absorption spectra of the optimized Al/TiO_2/AlN structure with $h_2 = 17$ nm. We neglected the transmitted light and defined it as the absorption $A = 100 - R$, because a sufficiently thick Al substrate reflects most of the light and attenuates the transmitted light to zero. The solid curves and open circles indicate the Fresnel and FDTD-calculated spectra, respectively. Figure 5(a) exhibits excellent agreement between the spectra calculated using the Fresnel formula and FDTD. The spectra show that normal reflection from $\lambda = 250$ to 300 nm was highly suppressed, and the average reflectivity was less than 1.98%.

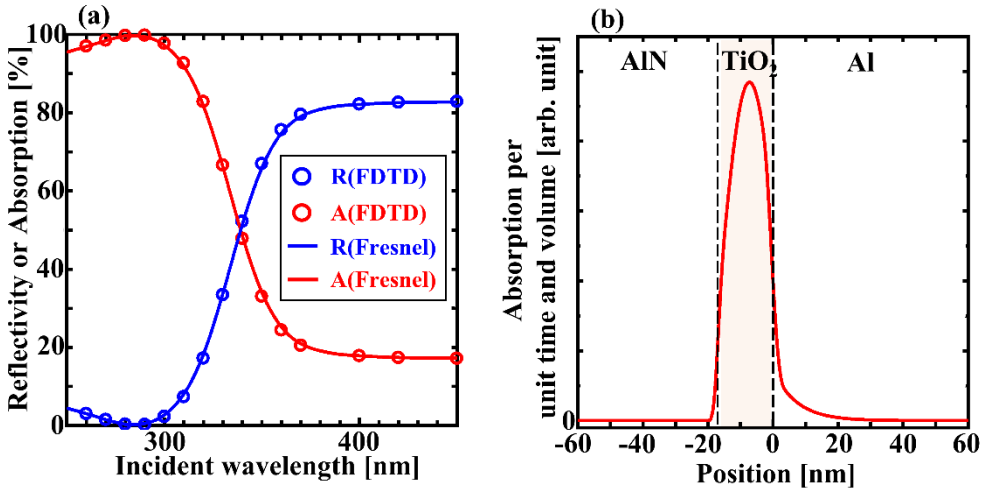

Fig. 5. (a) Calculated normal reflection and absorption of the designed Al/TiO_2/AlN. The thickness of TiO_2 is 17 nm. (b) Distribution of absorption per unit time and volume ($\lambda = 290$ nm).

Optics EXPRESS

This low reflectivity provides high absorption (> 95% at $\lambda = 250$–300 nm), with a maximum of 99.8%. Figure 5(b) shows the spatial distribution of the absorption per unit time and volume under the highest absorption condition. The spatial distribution indicates that most of the light is absorbed into the ultra-thin 17 nm TiO_2 layer, although the light penetrated slightly into Al. Thus, the DUV absorption predominantly originates from a TiO_2 layer that is much thinner than the wavelength. Light absorption into ultra-thin planar absorbers is of considerable benefit from the perspective of the high photocurrent density generation of the photodetector.

3. Results and discussion

An optimized Al/TiO_2/AlN system was fabricated on a c-sapphire substrate. Figure 6 shows the schematic of the sample. To obtain a high-quality thick AlN layer, we employed a metalorganic vapor-phase epitaxy technique [41]. The thickness of the grown AlN layer was approximately 2.7 μm. Ultra-thin TiO_2 and thick Al films were deposited by electron beam evaporation at a chamber pressure of 3×10^{-4} Pa. The sapphire substrate was then mechanically polished to obtain a specular surface. A scanning electron microscopy (SEM) image of the cross-section of the fabricated sample is shown in Fig. 7. Figure 7(a) shows the overall view of the fabricated Al/TiO_2/AlN sample on the sapphire substrate. Figure 7(b) shows an enlarged image near the TiO_2/AlN interface. The thicknesses of the evaporated Al and TiO_2 were approximately 100 and 17 nm, respectively.

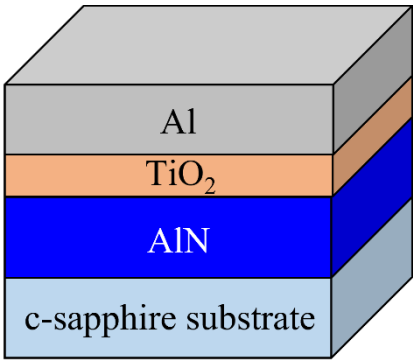

Fig. 6. Schematic of the fabricated sample of Al/TiO_2/AlN.

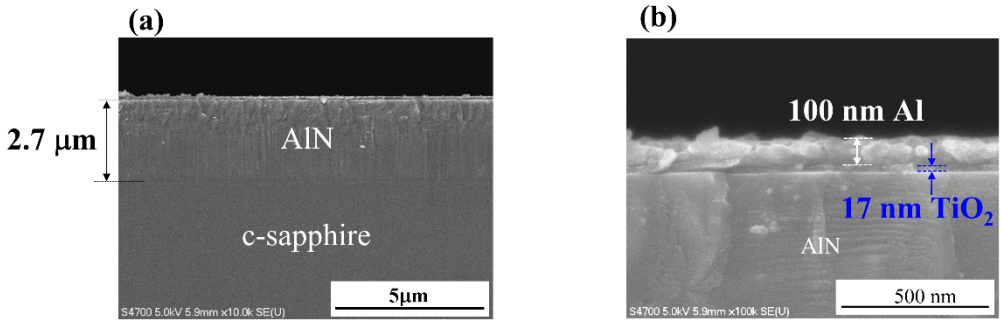

Fig. 7. (a) SEM image of the overall fabricated Al/TiO_2/AlN sample on c-sapphire. (b) Enlarged SEM image near the Al-TiO_2 interface.

Optics EXPRESS

The absorber performance of the fabricated sample was measured. Figure 8 shows the measurement system used to evaluate the absorption characteristics of the sample. A light-emitting diode (LED) with a peak wavelength of 265 nm and full width half maximum of 14 nm was used as the light source. The LED emission propagated along the optical fiber and normally entered the fabricated sample from the polished sapphire side.

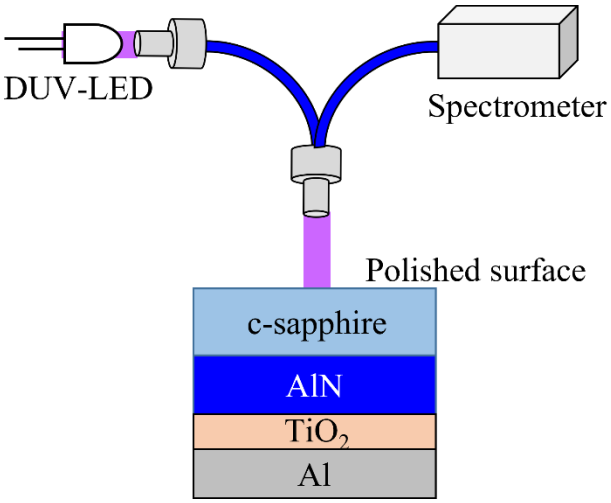

Fig. 8. Measurement system for reflection spectra of the fabricated sample.

The reflected light intensity was measured using a spectrometer (Flame, Ocean Photonics Co.). The measured reflection, transmission, and absorption spectra are shown in Fig. 9. We verified that the intensity of the transmitted light through the sample was significantly attenuated and vanished, as shown in Fig. 9 (green solid line). Thus, we defined the absorption of the sample as the 100-reflectivity. The sample 's reflectivity was evaluated using a commercial dielectric multilayer mirror for DUV (TFMS-25.4C05-2/4, Sigma Co.).

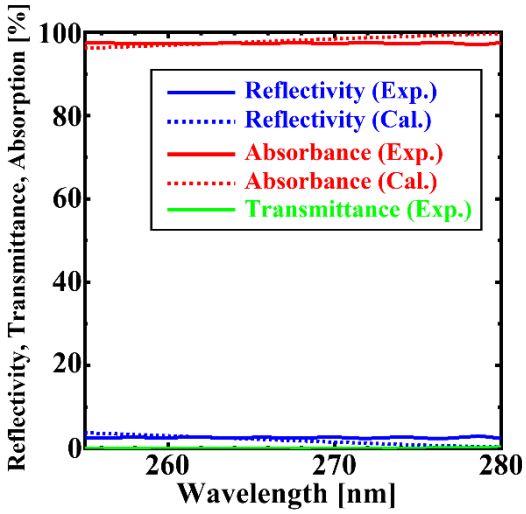

Fig. 9. Measured reflection, transmission, and absorption spectra of the fabricated sample. The solid and dashed lines represent experimental and calculated results, respectively.

Optics EXPRESS

The solid and dashed lines (blue and red) in Fig. 9 represent the experimental and calculated spectra, respectively. The reflection was highly suppressed in the wavelength range from 255 to 280 nm, and the average of the experimental reflectivity was less than 3%. As a result, the fabricated sample absorbed 97.4% of the incident light on average, and with maximum absorption of 97.6% at $\lambda = 276$ nm. The measured reflection and absorption characteristics of the sample exhibited good agreement with the Fresnel calculations. The results indicate that our sample achieves absorption performance comparable to other reports, despite the thickness of the lossy film being less than $\lambda/10$ [27,32,37]. Near-perfect absorption into ultra-thin lossy films is of great use for several applications, such as highly sensitive DUV photodetectors, because the small volume of the absorption film assists in generating a high-density photocurrent. Moreover, our structure does not require complex or costly nanofabrication processes. This ease of fabrication makes it suitable for low-cost and large-area manufacturing.

The measured absorption spectra differ slightly from the calculated spectra. We attribute this deviation to the fluctuation of the refractive index of the evaporated TiO_2 film. TiO_2 has polymorphs such as rutile, anatase, and amorphous, whose refractive index values are significantly different. The formation of these phases depends sensitively on the deposition conditions [42]. Hence, we can consider that the fluctuation of the refractive index causes a difference between the measured and calculated absorption characteristics. To verify this hypothesis, we estimated the influence of the TiO_2 refractive index fluctuation on the absorption spectra of our structure (the calculation model is $h_2 = 17$ nm in Fig. 1).

Figure 10 shows the calculated influence of the TiO_2 refractive index on the absorption spectra of AlN/17 nm TiO_2/Al. The real and imaginary parts of the TiO_2 refractive index fluctuation (Δn_{TiO2} and Δk_{TiO2}) are defined as the deviation from the values used in the design section (the value was taken from the experimental results of Siefke et al. [23]). The Δn_{TiO2} and Δk_{TiO2} values were assumed to vary up to 0.2, because this value was previously reported as a typical difference in the refractive index between rutile and anatase TiO_2 [42]. As shown in Fig. 10(a), increasing Δk_{TiO2} causes a decrease in absorption at all wavelengths, but the shape of the spectrum does not change. However, Fig. 10(b) shows that increasing Δn_{TiO2} weakens the difference in absorption at each wavelength, and the spectra flatten as Δn_{TiO2} increases. This calculated tendency explains the experimental absorption spectra. Also, the experimental absorption spectrum contains the effect of interference of AlN and sapphire substrate because the crystal growth of high quality AlN requires the sapphire substrate. We calculated and estimated the effect of interference in the sapphire and AlN. For example, the interference causes a 3% decrease of the absorption at 280 nm wavelength, assuming the 400 μm and 2.7 μm sapphire and AlN, respectively. The consideration clarifies that removing the sapphire substrate can improve absorption performance. In further work, we will try to demonstrate the higher performance of the DUV absorber with self-standing AlN film.

We also show the incident angle dependence of absorption spectra of the fabricated sample in Fig. 11. The inset in Fig. 11 shows the schematic diagram of angle dependence measurement. The incident angle θ is defined by the propagation direction of the incident light (the light is unpolarized) and the surface normal. Figure 11 indicates that the absorption decreases with the increase of incident angle. The measured dependence reveals our sample maintains more than 90% absorption up to the incident angle of 30 degrees, and this incident angle allowance is useful for practical applications, such as DUV photodetectors.

Optics EXPRESS

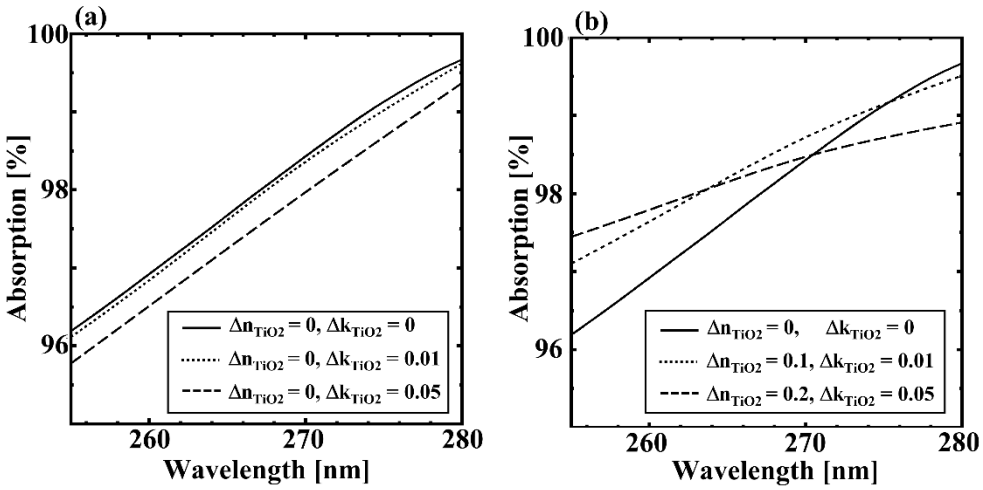

Fig. 10. Dependence of absorption spectra of the fabricated Al/TiO_2/AlN. (a) on Δk_{TiO2} (b) on both Δn_{TiO2} and Δk_{TiO2}.

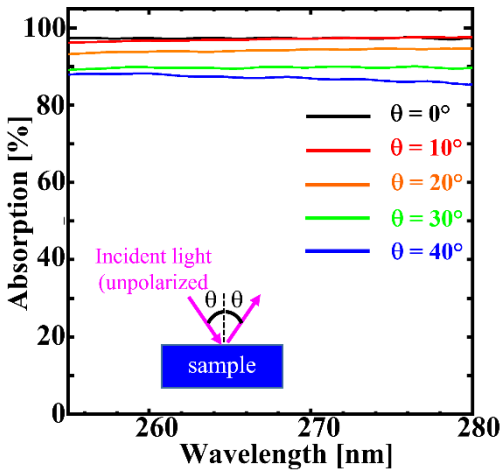

Fig. 11. Angular dependence of the absorption spectra of the fabricated sample. The inset is a schematic diagram of the measurement.

Optics EXPRESS

4. Conclusion

We demonstrated a near-perfect DUV absorber using multi-interference in an Al/TiO_2/AlN system. The Fresnel coefficient phasor diagram of the optimized system indicates that T and R vanish owing to the relaxed refractive index contrast at the TiO_2-AlN interface. Moreover, the FDTD field calculation clarified that almost all the light energy was absorbed into a TiO_2 film that is much thinner than the wavelength. We fabricated the optimized structure, and the measured average absorption of the fabricated sample reached 97.4% at wavelengths of 255–280 nm. The near-perfect absorption of ultra-thin TiO_2 films is of great use for several applications, such as generating high-density photocurrents in DUV photodetectors. In addition, our structure does not require costly or complicated nanopatterning processes, and its ease of fabrication is advantageous for low-cost and large-area manufacturing.

Funding. Japan Society for the Promotion of Science KAKENHI (JP21K14515).

Acknowledgments. The authors thank C. Azuma and S. Sugano of Tokushima University for their technical support with the SEM measurements.

Disclosures. The authors declare no conflicts of interest.

Data availability. The data underlying the results presented in this paper are not publicly available at this time, but may be obtained from the authors upon reasonable request.

References

1. H. Amano, R. Collazo, and C. De Santi, *et al.*, "The 2020 UV emitter roadmap," J. Phys. D: Appl. Phys. **53**(50), 503001 (2020).
2. W. Weng, M. Aldén, and Z. Li, "Quantitative SO_2 detection in combustion environments using broad band ultraviolet absorption and laser-induced fluorescence," Anal. Chem. **91**(16), 10849–10855 (2019).
3. M. E. Hughes, E. Brandin, and J. A. Golovchenko, "Optical absorption of DNA-carbon nanotube structures," Nano Lett. **7**(5), 1191–1194 (2007).
4. C. A. Gueymard, "Parameterized transmittance model for direct beam and circumsolar spectral irradiance," Sol. Energy **71**(5), 325–346 (2001).
5. N. I. Landy, S. Sajuyigbe, J. J. Mock, D. R. Smith, and W. J. Padilla, "Perfect metamaterial absorber," Phys. Rev. Lett. **100**(20), 207402 (2008).
6. H. Tao, N. I. Landy, C. M. Bingham, X. Zhang, R. D. Averitt, and W. J. Padilla, "A metamaterial absorber for the terahertz regime: Design, fabrication and characterization," Opt. Express **16**(10), 7181–7188 (2008).
7. I. Faniayeu and V. Mizeikis, "Vertical split-ring resonator perfect absorber metamaterial for IR frequencies realized via femtosecond direct laser writing," Appl. Phys. Express **10**(6), 062001 (2017).
8. R. Mudachathi and T. Tanaka, "3D conical helix metamaterial–based isotropic broadband perfect light absorber," Opt. Express **27**(19), 26369–26376 (2019).
9. J. Hao, J. Wang, X. Liu, W. J. Padilla, L. Zhou, and M. Qiu, "High performance optical absorber based on a plasmonic metamaterial," Appl. Phys. Lett. **96**(25), 251104 (2010).
10. C. Wu, B. Neuner, G. Shvets, J. John, A. Milder, B. Zollars, and S. Savoy, "Large-area wide-angle spectrally selective plasmonic absorber," Phys. Rev. B **84**(7), 075102 (2011).
11. K. Aydin, V. E. Ferry, R. M. Briggs, and H. A. Atwater, "Broadband polarization-independent resonant light absorption using ultrathin plasmonic super absorbers," Nat. Commun. **2**(1), 517 (2011).
12. M. S. Mahmud, D. Rosenmann, D. A. Czaplewski, J. Gao, and X. Yang, "Chiral plasmonic metasurface absorbers in the mid-infrared wavelength range," Opt. Lett. **45**(19), 5372–5375 (2020).
13. W. Wang, Y. Qu, K. Du, S. Bai, J. Tian, M. Pan, H. Ye, M. Qiu, and Q. Li, "Broadband optical absorption based on single-sized metal-dielectric-metal plasmonic nanostructures with high-ε'' metals," Appl. Phys. Lett. **110**(10), 101101 (2017).
14. C. W. Cheng, M. N. Abbas, C. W. Chiu, K. T. Lai, M. H. Shih, and Y. C. Chang, "Wide-angle polarization independent infrared broadband absorbers based on metallic multi-sized disk arrays," Opt. Express **20**(9), 10376–10381 (2012).
15. F. Qin, X. Chen, Z. Yi, W. Yao, H. Yang, Y. Tang, Y. Yi, H. Li, and Y. Yi, "Ultra-broadband and wide-angle perfect solar absorber based on TiN nanodisk and Ti thin film structure," Sol. Energy Mater. Sol. Cells **211**, 110535 (2020).
16. A. Becheri, M. Dürr, P. Lo Nostro, and P. Baglioni, "Synthesis and characterization of zinc oxide nanoparticles: Application to textiles as UV-absorbers," J. Nanopart. Res. **10**(4), 679–689 (2008).
17. M. K. Hedayati, M. Javaherirahim, B. Mozooni, R. Abdelaziz, A. Tavassolizadeh, V. S. K. Chakravadhanula, V. Zaporojtchenko, T. Strunkus, F. Faupel, and M. Elbahri, "Design of a perfect black absorber at visible frequencies using plasmonic metamaterials," Adv. Mater. **23**(45), 5410–5414 (2011).
18. R. Yahiaoui, K. Hanai, K. Takano, T. Nishida, F. Miyamaru, M. Nakajima, and M. Hangyo, "Trapping waves with terahertz metamaterial absorber based on isotropic Mie resonators," Opt. Lett. **40**(13), 3197–3200 (2015).

Optics EXPRESS

19. X. Liu, Q. Zhao, C. Lan, and J. Zhou, "Isotropic Mie resonance-based metamaterial perfect absorber," Appl. Phys. Lett. **103**(3), 031910 (2013).
20. M. Miyata, H. Hatada, and J. Takahara, "Full-color subwavelength printing with gap-plasmonic optical antennas," Nano Lett. **16**(5), 3166–3172 (2016).
21. P. B. Johnson and R. W. Christy, "Optical constants of the noble metals," Phys. Rev. B **6**(12), 4370–4379 (1972).
22. D. E. Aspnes and A. A. Studna, "Dielectric functions and optical parameters of Si, Ge, GaP, GaAs, GaSb, InP, InAs, and InSb from 1.5 to 6.0 eV," Phys. Rev. B **27**(2), 985–1009 (1983).
23. T. Siefke, S. Kroker, K. Pfeiffer, O. Puffky, K. Dietrich, D. Franta, I. Ohlídal, A. Szeghalmi, E. B. Kley, and A. Tünnermann, "Materials Pushing the Application Limits of Wire Grid Polarizers further into the Deep ultraviolet Spectral Range," Adv. Opt. Mater. **4**(11), 1780–1786 (2016).
24. W. Dallenbach and W. Kleinsteuber, "Reflection and absorption of decimeter-waves by plane dielectric layers," Hochfrequenztech. Elektroakustik **51**, 152–156 (1938).
25. H. Bosman, Y. Y. Lau, and R. M. Gilgenbach, "Microwave absorption on a thin film," Appl. Phys. Lett. **82**(9), 1353–1355 (2003).
26. C. Hägglund, S. P. Apell, and B. Kasemo, "Maximized optical absorption in ultrathin films and its application to plasmon-based two-dimensional photovoltaics," Nano Lett. **10**(8), 3135–3141 (2010).
27. Z. Li, E. Palacios, S. Butun, H. Kocer, and K. Aydin, "Omnidirectional, broadband light absorption using large-area, ultrathin lossy metallic film coatings," Sci. Rep. **5**(1), 15137 (2015).
28. A. Monti, A. Toscano, and F. Bilotti, "Exploiting the surface dispersion of nanoparticles to design optical-resistive sheets and Salisbury absorbers," Opt. Lett. **41**(14), 3383–3386 (2016).
29. C. S. Park and S. S. Lee, "Narrowband and flexible perfect absorber based on a thin-film nano-resonator incorporating a dielectric overlay," Sci. Rep. **10**(1), 17727 (2020).
30. K. V. Sreekanth, R. Medwal, Y. K. Srivastava, M. Manjappa, R. S. Rawat, and R. Singh, "Dynamic Color generation with electrically tunable thin film optical coatings," Nano Lett. **21**(23), 10070–10075 (2021).
31. M. A. Kats, D. Sharma, J. Lin, P. Genevet, R. Blanchard, Z. Yang, M. M. Qazilbash, D. N. Basov, S. Ramanathan, and F. Capasso, "Ultra-thin perfect absorber employing a tunable phase change material," Appl. Phys. Lett. **101**(22), 221101 (2012).
32. J. Park, J. H. Kang, A. P. Vasudev, D. T. Schoen, H. Kim, E. Hasman, and L. M. Brongersma, "Omnidirectional near-unity absorption in an ultrathin planar semiconductor layer on a metal substrate," ACS Photonics **1**(9), 812–821 (2014).
33. J. Park, S. J. Kim, and M. L. Brongersma, "Condition for unity absorption in an ultrathin and highly lossy film in a Gires–Tournois interferometer configuration," Opt. Lett. **40**(9), 1960–1963 (2015).
34. M. A. Kats, R. Blanchard, P. Genevet, and F. Capasso, "Nanometre optical coatings based on strong interference effects in highly absorbing media," Nat. Mater. **12**(1), 20–24 (2013).
35. M. A. Kats and F. Capasso, "Optical absorbers based on strong interference in ultra-thin films," Laser Photonics Rev. **10**(5), 735–749 (2016).
36. V. Medvedev, V. Gubarev, E. Zoethout, and N. Novikova, "Interference-enhanced absorption of visible and near-infrared radiation in ultrathin film coatings," IEEE Photonics Technol. Lett. **33**(22), 1242–1245 (2021).
37. K. T. Lee, C. Ji, and L. J. Guo, "Wide-angle, polarization-independent ultrathin broadband visible absorbers," Appl. Phys. Lett. **108**(3), 031107 (2016).
38. M. ElKabbash, T. Letsou, S. A. Jalil, N. Hoffman, J. Zhang, J. Rutledge, A. R. Lininger, C. H. Fann, M. Hinczewski, G. Strangi, and C. Guo, "Fano-resonant ultrathin film optical coatings," Nat. Nanotechnol. **16**(4), 440–446 (2021).
39. A. D. Rakić, "Algorithm for the determination of intrinsic optical constants of metal films: Application to aluminum," Appl. Opt. **34**(22), 4755–4767 (1995).
40. J. Pastrňák and L. Roskovcová, "Refraction index measurements on AlN single crystals," Phys. Status Solidi B **14**(1), K5–K8 (1966).
41. K. Nagamatsu, S. Tsuda, T. Miyagawa, R. Aono, H. Hirayama, Y. Takashima, and Y. Naoi, "Reduction of parasitic reaction in high-temperature AlN growth by jet stream gas flow metal-organic vapor phase epitaxy," Sci. Rep. **12**(1), 7662 (2022).
42. K. Möls, L. Aarik, H. Mändar, A. Kasikov, A. Niilisk, R. Rammula, and J. Aarik, "Influence of phase composition on optical properties of TiO2: Dependence of refractive index and band gap on formation of TiO2-II phase in thin films," Opt. Mater. **96**, 109335 (2019).